Ceramics International 50 (2024) 4632–4639

Contents lists available at ScienceDirect

Ceramics International

journal homepage: www.elsevier.com/locate/ceramint

Photoluminescence and EPR spectroscopic studies on narrowband ultraviolet-B (NB-UVB) emitting trivalent gadolinium-doped $CaAl_4O_7$ material for phototherapy lamps

Vijay Singh [a,*,1], Jung-Kul Lee [a,1], M. Seshadri [b], Aadil Ahmad Bhat [a], S. Watanabe [c], T.K. Gundu Rao [c]

[a] Department of Chemical Engineering, Konkuk University, Seoul, 05029, Republic of Korea
[b] Department of Physics, Koneru Lakshmaiah Education Foundation, Hyderabad, 500043, Telangana, India
[c] Institute of Physics, University of Sao Paulo, SP, 05508-090, Brazil

ARTICLE INFO

Handling Editor: Dr P. Vincenzini

Keywords:
Sol-gel
EPR
Gd^{3+} ions
$CaAl_4O_7$
Ultraviolet-B

ABSTRACT

Using the sol-gel process, a series of Gd^{3+} doped $CaAl_4O_7$ samples were fabricated. Their crystal characteristics, surface morphologies, and spectral characteristics were analyzed using X-ray powder diffraction (XRD), Fourier transform infrared (FTIR), scanning electron microscopy (SEM), and photoluminescence (PL) spectroscopy. XRD analysis reveals that the prepared phosphor exhibits a single monoclinic phase, indicating a well-defined crystal lattice. Under the excitation wavelength of 272 nm, weak and strong emission peaks were identified at 307 nm and 314 nm, which correspond to $^6P_{5/2} \rightarrow {}^8S_{7/2}$ and $^6P_{7/2} \rightarrow {}^8S_{7/2}$ transitions, respectively. A strong electron paramagnetic resonance (EPR) signal of the $CaAl_4O_7$:Gd^{3+} phosphor was observed at $g_{eff} \sim 2.16$ and 1.94 along with several weak EPR signals that were observed at $g_{eff} \sim 14.8$, 9.7, 5.6, 4.8, 3.7, 3.16, 2.7 and 1.5. The intense narrowband at 314 nm in the ultraviolet-B region makes prepared phosphor a promising candidate for phototherapy lamp applications. This study presents a comprehensive investigation of the Gd^{3+} doped $CaAl_4O_7$ phosphor, addressing its structural, and luminescent properties, which contributes to a deeper understanding of this material for various technological applications.

1. Introduction

Over the past few decades, inorganic phosphor materials have been widely used in a variety of applications such as white LEDs, field emission displays, high-definition television screens, X-ray imaging, biomarkers, bioimaging, luminescent electrodes, and ceramics which encouraged researchers to search for novel materials with useful properties [1–4]. CaO-Al_2O_3 (CA)-based binary inorganic systems have been the subject of many studies in recent years due to their superior thermal characteristic for the use in high-temperature refractories [5,6]. They also play significant roles in cement technology as hydraulic materials and metallurgical slags in the steel sector. In fact, the CA compound system exhibits three main phases, $CaAl_2O_4$, $CaAl_4O_7$, and $Ca_{12}Al_{14}O_{33}$ in the phase diagram. All three phases show emerging applications in various fields including material science and ceramic technology. The $CaAl_4O_7$ host matrix receives special interest from researchers due to its unique crystallographic characteristics and a high melting point of about 1765 ± 25 °C. Among all high-alumina cement, $CaAl_4O_7$ is largely recommended for usage and is a highly valuable chemical, especially in casting, trowelling, and gunning applications. $CaAl_4O_7$ is used as a high-temperature ceramic for refractory applications. Wu et al. [7] prepared a low permittivity $CaAl_4O_7$ ceramics by solid-state reaction method and systematically reported its structural, vibrational, and microwave dielectric properties.

$CaAl_4O_7$, with its monoclinic crystal structure, high chemical stability, and endurance, is an excellent carrier of optical material for phosphors [8]. Doping is an effective way to modulate the properties of any crystal lattice without changing its primary structure. In recent decades, much research has been done on the doping of rare earth (REs) ions and transition metal (TMs) ions for use in a variety of scientific and practical applications, such as lighting, display technologies, communications, detectors, security, etc. Due to their high quantum efficiency,

* Corresponding author.
E-mail address: vijayjiin2006@yahoo.com (V. Singh).
[1] These authors contributed equally to this work.

https://doi.org/10.1016/j.ceramint.2023.11.207
Received 22 August 2023; Received in revised form 30 October 2023; Accepted 16 November 2023
Available online 19 November 2023
0272-8842/© 2023 Elsevier Ltd and Techna Group S.r.l. All rights reserved.

prolonged phosphorescence persistence, and appropriate emission hue, oxide-based phosphors doped with rare-earth elements (Ce, Tb, Sm, and Eu) have received a lot of interest [9–14]. Jia et al. [15] prepared $CaAl_4O_7:Tb^{3+}$, Ce^{3+} by sintering, and luminescence features were reported for displays requiring blue emission. Kumar et al. [16] investigated the blue light-emitting $CaAl_4O_7:Tm^{3+}$ phosphors prepared by the conventional Pechini sol-gel method. Puchalska et al. [17] studied the luminescent kinetics of Eu^{3+} ions in $CaAl_4O_7:Eu^{3+}$ prepared by the Pechini method. Park et al. [18] reported structural and red-emitting $CaAl_4O_7:Mn^{4+}$ phosphors. Singh et al. [19] investigated the photoluminescence properties of $CaAl_4O_7:Tb^{3+}$ phosphors for display panel applications. $CaAl_4O_7$ materials have been synthesized using a variety of techniques, including combustion, coprecipitation, and hydrothermal processing. On the other hand, the sol-gel method offers several advantages, including precise composition control, homogeneity, and low-temperature processing [20–22].

Most efforts can be directed toward the development of display technologies that use $CaAl_4O_7$ phosphor-containing REs or TMs to produce visible light. In this work, we are interested in ultraviolet light with $CaAl_4O_7:Gd^{3+}$ phosphor for phototherapy lamps. Normally, the spectral region from 100 to 380 nm is ultraviolet (UV) radiation, which is invisible. Among the known ultraviolet -A, -B, and -C regions, UV-B is the most beneficial operational radiation for the treatment of skin-related health issues and disorders. The use of gadolinium (Gd^{3+}) as an activator for a variety of host matrices has shown promising therapeutic results, and Gd is one of the most significant lanthanide ions due to the narrowband ultraviolet-B (NB-UVB) emission in the range of 310–320 nm (Gd^{3+}: $^6P_J \rightarrow {}^8S_{7/2}$).

Gd^{3+} behaves as an active ion in several host lattices ($CaAl_{12}O_{19}$, ZnO, $YScO_3$, $MgAl_2O_4$, etc.) and their optical characteristics are described [23–26]. EPR studies have also been carried out on some of the phosphors like $Y_4Zr_3O_{12}:Gd^{3+}$ [27], $GdAlO_3$ [28], and $EuAl_3(BO_3)_4:Gd^{3+}$ [29]. In the current investigation, we have carried out a thorough analysis of Gd^{3+}-activated $CaAl_4O_7$ phosphors, which have been synthesized through the sol-gel method at relatively low temperatures. The analysis encompasses the use of powder X-ray diffraction (XRD), scanning electron microscopy (SEM), electron paramagnetic resonance (EPR), and photoluminescence techniques.

2. Materials preparation and analysis

The sol-gel technique is a versatile and widely used method for the synthesis of various materials, including ceramics, glasses, and nanoparticles. The sol-gel technique allows for precise control over the composition and structure of the synthesized materials. The described sol-gel process in this study is a well-established and effective method for the preparation of high-quality materials with tunable properties. In this investigation, using the sol-gel technique, a series of $CaAl_4O_7:Gd^{3+}$ (CA1-CA7) phosphors depending on the concentration of Gd^{3+} ions were synthesized. High-quality analytical-grade raw materials were used to prepare $CaAl_4O_7:Gd^{3+}$ phosphor powder. Compositional information for the preparation of $CaAl_4O_7:Gd^{3+}$ phosphor is shown in Table 1. In a typical synthesis, a molar ratio of 2:1, citric acid and metal ions ($CaX_2•4H_2O$, $AlX_3•9H_2O$, $GdX_3•6H_2O$ in which X = (NO_3)) were first dissolved in deionized water with constant stirring and heating for about 60 min at 80 °C, then kept in an oven at 110 °C to obtain uniform dried gels. The solid gel is then heated at 400 °C for 120 min to obtain powder, which appears brownish due to carbon residuals. Finally, the resulting brownish powder is thoroughly ground and sintered at 1000 °C for 180 min in air. A schematic presentation of the synthesis is shown in Fig. 1.

Table 1
Detailed information on sample composition and starting materials.

Sample composition	Sample code	Starting materials (in grams)			
		Ca (× 10^{-4})	Al	C.A (× 10^{-4})	Gd (× 10^{-4})
$CaAl_4O_7$:0.005Gd	CA1	4722	3	38420	45
$CaAl_4O_7$:0.015Gd	CA2	4722	3	38420	135
$CaAl_4O_7$:0.030Gd	CA3	4722	3	38420	270
$CaAl_4O_7$:0.045Gd	CA4	4722	3	38420	406
$CaAl_4O_7$:0.060Gd	CA5	4722	3	38420	541
$CaAl_4O_7$:0.075Gd	CA6	4722	3	38420	676
$CaAl_4O_7$:0.090Gd	CA7	4722	3	38420	812

[Ca= $Ca(NO_3)_2•4H_2O$, Al= $Al(NO_3)_3•9H_2O$, C.A = Citric acid, Gd=Gd $(NO_3)_3•6H_2O$].

The XRD pattern of the sample powders was recorded at a scan rate of 5°/minute over a range of 10–80° of a 2θ scale using an X-ray diffractometer (RIGAKU Miniflex-II) consisting of CuKα (λ = 1.5406 Å) and operating at 40 kV and 30 mA for all samples. The morphological photographs were taken with the S-3400, Hitachi - Japan electron microscope. To identify the functional group present in prepared samples; Fourier transform infrared (6700, Thermo Fisher Nicolet) spectrometer operated in the range of 400–4000 cm^{-1} was used. The photoluminescence spectra were recorded with an RF-5301PC SHIMADZU fluorophotometer, which contains a Xenon lamp as an excitation. An ESR Spectrometer (JEOL FE1X) was used to record EPR spectra with a field modulation of 100 kHz.

3. Results and discussion

3.1. X-ray diffraction

Fig. 2 shows the X-ray diffraction pattern of $CaAl_4O_7$ and $CaAl_4O_7:Gd^{3+}$ (CA1-CA7) phosphors. All samples exhibit a similar XRD pattern. The prepared samples belong to the monoclinic phase of $CaAl_4O_7$ with C2/c space symmetry which matches closely to the JCPDS card no. 23-1037. The crystal structure representation of the pristine and Gd-modified phosphor is shown in Fig. 3. The crystallite size and lattice strain are determined from the observed diffraction peaks by the well-known Scherrer equation.

$$d = 0.9\lambda/\beta \cos\theta \quad (1)$$

where d is the crystalline grain size, 0.9 is the shape factor, λ is the wavelength (1.5406 Å), θ is the Bragg angle and β is the diffracted full width at half-maximum (FWHM). Table 2 presents the FWHM, crystallite size and lattice strain for all samples. The mean size of crystallites for the studied systems is around 27-34 nm. As the concentration of Gd increases in the crystal lattice, the XRD peak position shifts towards a higher value of 2θ due to the difference in ionic radius. The size mismatch leads to local lattice distortions which results in the increase in lattice strain. A shift in the higher side of 2θ typically indicates a change in the crystal structure or lattice spacing of the material. A shift to higher 2θ values can lead to greater separation between diffraction peaks, resulting in improved resolution. This is particularly valuable while discussing its complex structure with closely spaced diffraction lines, as it allows for better discrimination between different crystalline phases.

3.2. SEM

The morphology of the $CaAl_4O_7:Gd^{3+}$ (CA3) sample is displayed in Fig. 4. The sample shows a plate-like morphology having particle size in micrometers. An additional factor affecting the crystal formation is the presence of Gd^{3+} ions as dopants. $CaAl_4O_7:Gd^{3+}$ crystal structure may favor growth along certain crystallographic planes, resulting in a flattened, plate-like phase. In $CaAl_4O_7:Gd^{3+}$ crystals, the growth rate in the direction perpendicular to the plate-like morphology may be higher, depending on the growth conditions and the inclusion of Gd^{3+} ions, which leads to plate-like crystal morphology. The shape and size of the particles are somewhat irregular. However, the particles facet had many ruptured traces and pores. Fig. 4B shows a magnified view of Fig. 4A

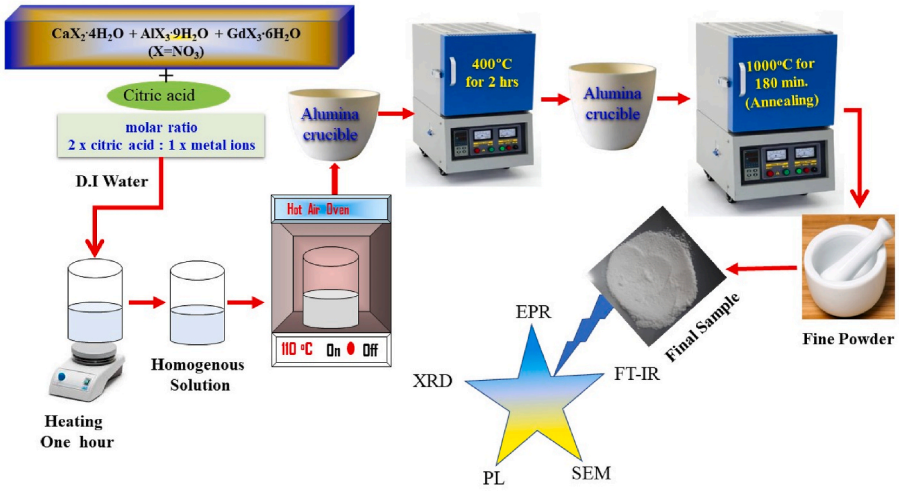

Fig. 1. Schematic diagram for the synthesis of $CaAl_4O_7$:Gd^{3+}.

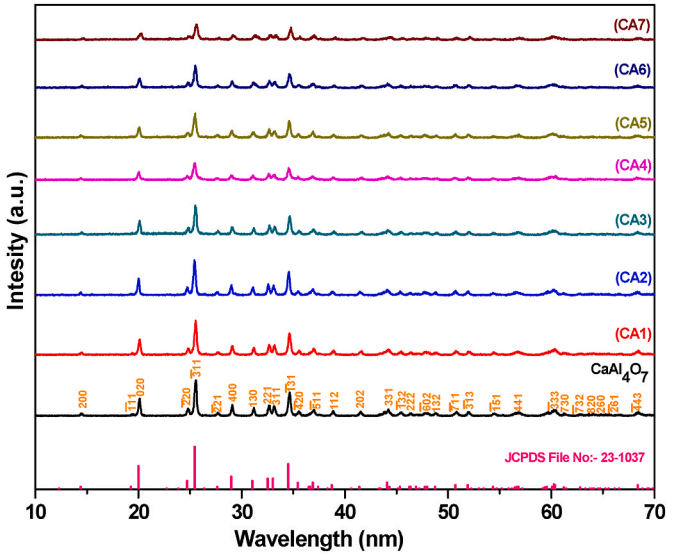

Fig. 2. Powder XRD pattern of $CaAl_4O_7$ and Gd^{3+}:$CaAl_4O_7$ (CA1-CA7) phosphors.

(zone a) where, at higher magnification of the image, there is a distinct porosity within the crystalline grains. This porosity is due to the evolution of large amount of gases during the sintering process. Fig. 4D shows a magnified view of Fig. 4C (zone C). Several small particles appear on the surface of the microparticles, which is caused by the evaporation of gas molecules under the influence of high pressure. The growth rate of a crystal can be influenced by the surface energy of different crystallographic faces. Depending on the crystallographic structure and the presence of certain ions of Gd^{3+}, the surface energy of specific faces may be reduced, promoting faster growth along those faces. This can result in plate-like crystal morphologies with faster growth in the perpendicular direction.

3.3. FT-IR, photoluminescence, and energy transfer analysis

Fig. 5 depicts the FT-IR spectrum of the sample used to determine the metal-oxygen vibrational frequency of $CaAl_2O_7$ nanoparticles. No large

Table 2
FWHM and crystallite size of Gd^{3+}:$CaAl_4O_7$ (CA1-CA7) phosphors.

Samples	Sample code	FWHM (Å)	Crystalline size (nm)	Lattice strain
$CaAl_4O_7$	–	0.2561	33.29	0.0050
$CaAl_4O_7$:0.005Gd	CA1	0.2742	31.04	0.0053
$CaAl_4O_7$:0.015Gd	CA2	0.2639	32.25	0.0051
$CaAl_4O_7$:0.030Gd	CA3	0.2560	33.25	0.0049
$CaAl_4O_7$:0.045Gd	CA4	0.3135	27.13	0.0061
$CaAl_4O_7$:0.060Gd	CA5	0.3106	27.40	0.0060
$CaAl_4O_7$:0.075Gd	CA6	0.2866	29.70	0.0055
$CaAl_4O_7$:0.090Gd	CA7	0.3137	27.13	0.0060

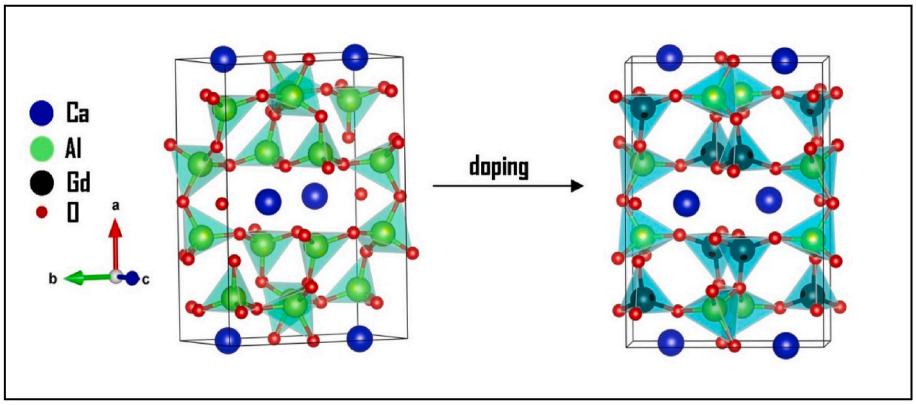

Fig. 3. Crystal structure of pristine and Gd-modified phosphor.

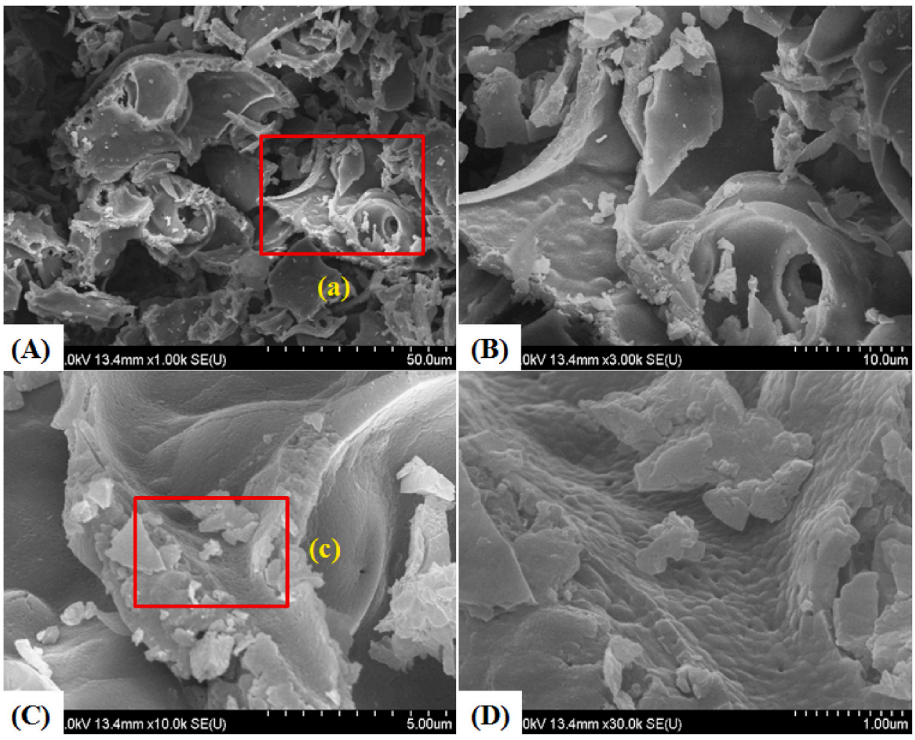

Fig. 4. SEM image, of Gd^{3+}:$CaAl_4O_7$ (CA3) phosphor.

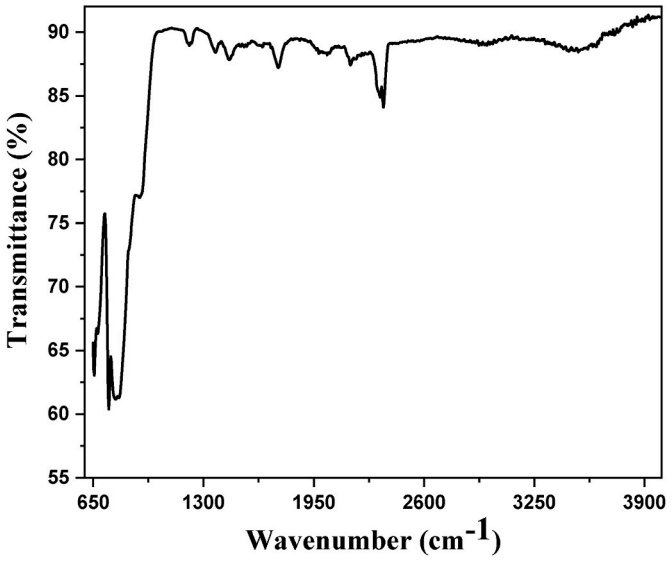

Fig. 5. FT-IR spectra of Gd^{3+}:$CaAl_4O_7$ (CA3) phosphor.

impurity peaks attributable to organic contaminants were found. The O-H band of water molecules is responsible for a broad peak at 3501 cm^{-1} [30]. However, a noticeable band can be visible at 2365 cm^{-1}, which is attributed to the C-H band stretching vibration. The peak at 2170 cm^{-1} is attributed to (N=N=N) azide stretching vibration. C-H bending peaks occur at 2015 and 1365 cm^{-1} [30]. Another minor peak at 1470 cm^{-1} is caused by the nitrate group. The existence of C-O stretching causes weak absorption at 1224 cm^{-1} [31,32]. The band at 1540 cm^{-1} indicates the presence of pollutants such as CO_2, which were probably absorbed from the air during the experiments. A special structural characteristic brought about by Gd doping may be shown by the absorption peak measured at 1356 cm^{-1} [33]. It could be connected to Gd-O vibrations, changes in the crystal structure brought on by the inclusion of Gd, or some other interaction involving Gd ions. A distinctive vibrational mode to the incorporation of Gd ions may be linked to the absorption peak at 1648 cm^{-1} [33]. This peak may be due to a vibrational mode associated with oxygen that is impacted by the presence of Gd. Gadolinium ions have frequently significant interactions with oxygen atoms in compounds and it might involve the stretching vibrations of Al-O or Ca-O bonds or changes in the crystal lattice brought on by the doping of Gd. The presence of a robust chemical bond or vibrational mode is suggested by the absorption peak at 1733 cm^{-1}. This vibration is due to the formation of a carboxylate group [34]. It could have something to do with carbon-oxygen (C-O) bonds or perhaps Gd-O bonds. The stretching vibration of M − O bonds (M = Ca, Al) can be attributed to the strong absorption bands at 813 cm^{-1} and 643 cm^{-1} [35]. The Gd_2O_3 ion is known to be an efficient light emitter in the ultraviolet (UV) and visible regions among the lanthanide group due to its intrinsic luminescence nature when irradiated under UV light. The low phonon energy and high Gd_2O_3 bandgap energy reduce multiphonon relaxation, which leads to enhanced radiative emission [36,37]. Moreover, the stretching and bending modes of the AlO_4 units are considerably high between 650 and 950 cm^{-1} in the FT-IR spectrum (see Fig. 5), which alleviates the non-radiative relaxation process to the emitting level ^6P_J (Gd^{3+}).

The photoluminescence excitation (PLE) and photoluminescence (PL) spectral measurements at ambient temperature in the region of 230~340 nm wavelength for $CaAl_4O_7$:Gd^{3+} phosphor samples, are depicted in Fig. 6 (a) and (b). The PLE exhibits well-resolved peaks of all samples monitored at the emission wavelength of 314 nm and is associated with the inter-configurational electronic transitions from the lowest level of $^8S_{7/2}$ to higher levels, (^6D_J, ^6P_J, ^6I_J, J = 7/2–17/2 region) around 243, 245, 252, 272, 275 and 278 nm, respectively [38]. Upon excitation, at a wavelength of 272 nm, strong and weak UV emission intensity appeared at 307 nm and 314 nm which is attributed to the $^6P_{5/2} \rightarrow {}^8S_{7/2}$ and $^6P_{7/2} \rightarrow {}^8S_{7/2}$ transitions of Gd^{3+}. In PLE and PL, the spectral intensities of all samples are maximally promoted with Gd^{3+} ions at 3 mol% and decrease the intensity of the $CaAl_4O_7$:Gd^{3+} phosphors with increasing Gd^{3+} dopant concentration to 9 mol%. Fig. 7 presents the emission intensity of the $^6P_{7/2} \rightarrow {}^8S_{7/2}$ (314 nm) peak

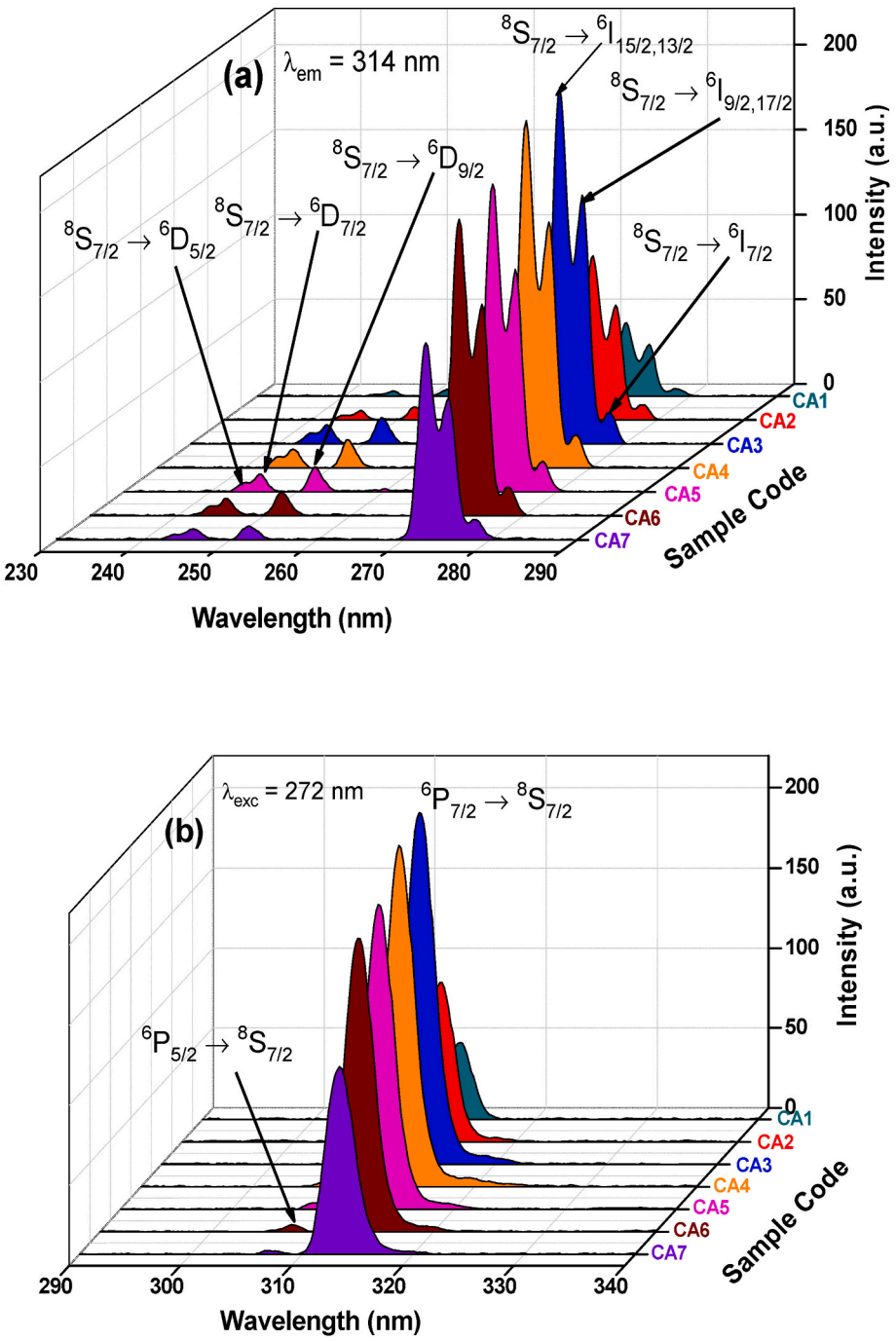

Fig. 6. Photoluminescence spectra of the Gd^{3+}:$CaAl_4O_7$ phosphor (a) Excitation spectrum of Gd^{3+}:$CaAl_4O_7$ (λ_{em} = 314 nm) and (b) Emission spectrum of Gd^{3+}:$CaAl_4O_7$ (λ_{exc} = 272 nm).

depending on the concentration of Gd ions. The increase in the Gd^{3+} ion concentration in the samples leads to a decrease in the emission intensity. In fact, the energy is transferred non-radiatively between the ions as the distance between the Gd^{3+} ions decreases with increasing concentration, so the concentration quenching effect plays a significant role in the luminescence mechanism. To know the possible energy transfer mechanism, an important parameter is the critical distance between Gd ion to Gd ion for transfer of energy (R_c), which is calculated from Blasse's formula [39],

$$R_c = 2\left[\frac{3V}{4\pi N X_c}\right]^{1/3} \quad (2)$$

where V is the cell size (=271.685 Å^3), N is the availability of cations in the unit cell (=4) and X_c is the optimal number of Gd^{3+} ions (=3 mol%). In this work, the estimated R_c is 8.14 Å, which shows that energy transfer through multipolar interactions leads to concentration quenching in Gd^{3+}:$CaAl_4O_7$ phosphors. The possible excitation and emission from electronic levels of Gd^{3+} ions are shown in Fig. 8.

According to Dexter's theory, the exact type of multiple interactions can be known since dipole-dipole (d↔d), dipole-quadrupole (d↔q), and quadrupole-quadrupole (q↔q) interactions occur between Gd^{3+} ions, using the following formula [35],

$$\frac{I}{x} = K\left\{1 + \beta(x)^{Q/3}\right\}^{-1} \quad (3)$$

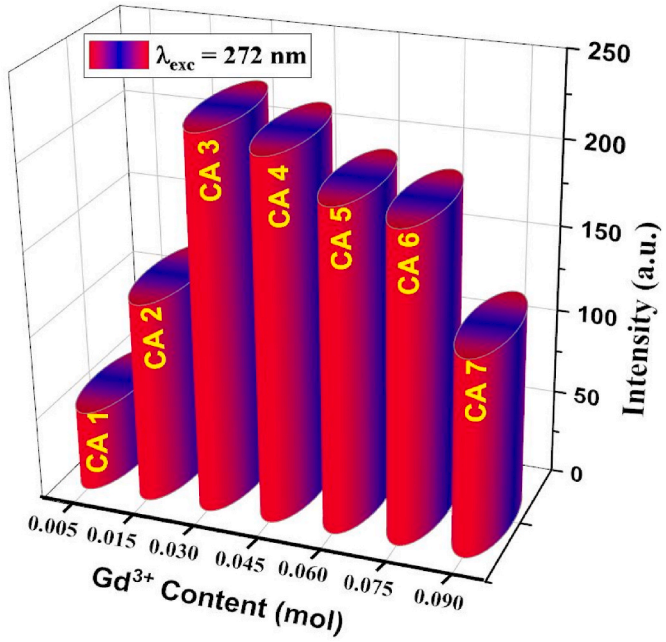

Fig. 7. Variation in the emission intensity of strong emission (314 nm) as a function of Gd^{3+} concentration.

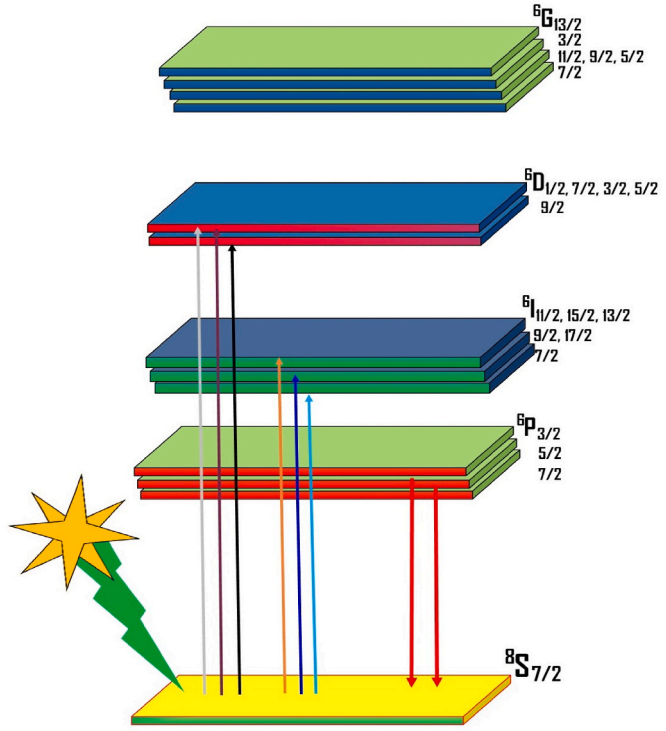

Fig. 8. Pictorial view describes the possible different electronic levels of Gd^{3+} ions.

where I is the intensity of the emission peak, x is the Gd concentration (3 mol%), K and β are the constants. Q is also a constant for the d↔d (6), d↔q (8), and q↔q (10) interactions. The estimated Q value in this work is 3.6 from the slope value of the linear fit to Log(I/x) versus Log(x) (see Fig. 9). The Q value suggests that the observed quenching of the emission intensity is taken into account due to the dipole-dipole interactions. The critical concentration of Gd^{3+} (3 mol%) containing $CaAl_4O_7$ phosphor may be useful in NB-UVB phototherapy lamps. When it comes to treating a range of skin diseases, phototherapy employing NB-UVB has been found to be more effective than traditional broadband UVB (BB-UVB).

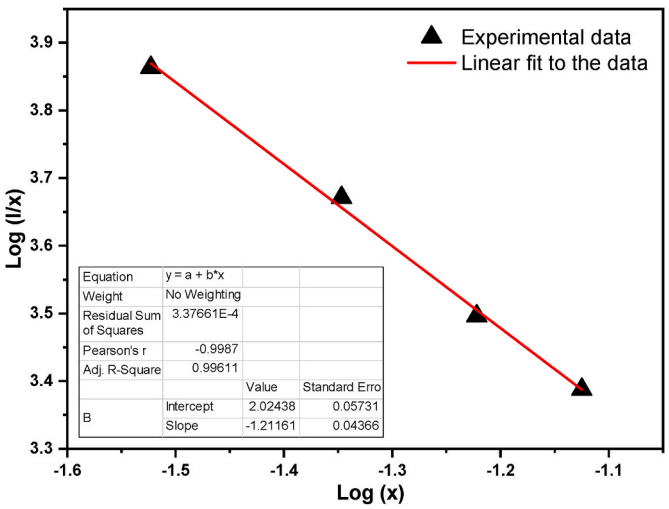

Fig. 9. Plot of Log (I/x) Vs Log (x) in Gd^{3+}:$CaAl_4O_7$ phosphor.

3.4. EPR spectral analysis

The EPR spectral lines of a representative CA7 sample recorded at room temperature are depicted in Fig. 10. Relatively strong lines are seen at g_{eff} ~2.16 and 1.94. On the other hand, the low-field spectral part saw more weak lines at g_{eff} ~14.8, 9.7, 5.6, 4.8, 3.7, 3.16, 2.7, and 1.5, respectively. Of the RE ions, the Eu^{2+} and Gd^{3+} ions have L = 0 with the electronic configuration [Xe]$4f^7$. When these ions are located in the crystal lattice, crystal field effects are negligible as they are S-state ions. However, higher-order distortions arise due to the spin-orbit coupling, which causes observable crystal field effects. Higher levels of L ≠ 0 are mixed with the lowest level and allow ions to interact in a crystal field environment. Generally, the site symmetry of Gd^{3+} ions is determined by the nearest neighboring ions. Therefore, changing the location of these neighboring ions leads to a change in the surrounding environment of the Gd^{3+} ions. This surrounding environment significantly alters the crystal field and there will be changes in the observed EPR spectra. In the specific case of disordered systems like glasses, a unique 'U shape spectrum' of EPR spectral lines is observed with lines at about g_{eff} ~2.0,

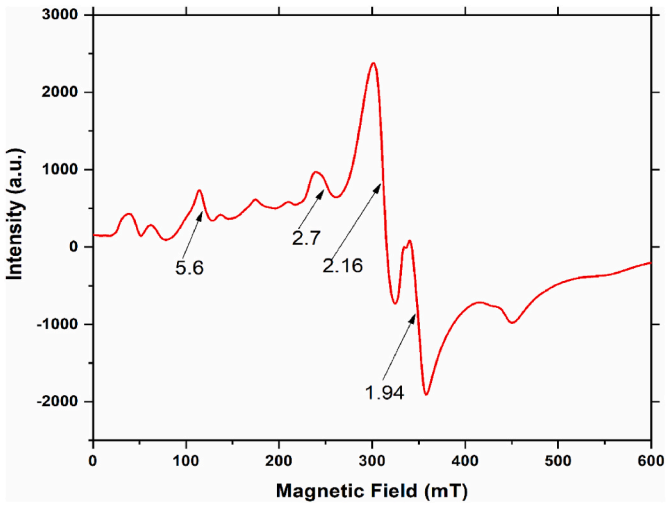

Fig. 10. Room temperature EPR spectrum of Gd^{3+}:$CaAl_4O_7$ phosphor.

2.8, and 5.9 due to the distribution of Gd^{3+} ions around the crystal filed environment [40,41].

$CaAl_4O_7$ has a grossite structure and crystallizes in the monoclinic phase of the C2/c group with lattice constants: $a = 12.86$ Å, $b = 8.879$ Å and $c = 5.44$ Å [42]. The calcium ion is located in a coordination sphere with 7-fold C_2 symmetry. The nearest neighboring oxygen ions are located at a distance that varies from 2.33 Å to 2.88 Å. There are two non-equivalent Al sites, and the Al ions are in the centre of the tetrahedral oxygen ions, which are closer to the principal tetrahedra. In $CaAl_4O_7$, sheets of corner-sharing AlO_4 tetrahedra are enlarged in the y and z directions, while Ca atoms are occupied between the sheets.

The EPR signal of the Gd^{3+} ion for powder samples was observed and discussed by Brodbeck and Iton [43]. They consider the magnitude of crystal field interaction (H_{CF}) and Zeeman splitting hν (where ν is the microwave frequency). They identified weak, intermediate, and strong regions in the EPR spectrum based on the $H_{CF}/h\nu$ ratio. The region, where $H_{CF}/h\nu \leq ¼$, is considered weak ($g \sim 2.0$). In the intermediate region of the EPR spectrum, a wide range of g values between 2.0 and ∞ (Lower) and g values greater than 2.0 (Higher) are expected. When the surroundings of the Gd^{3+} ion are not distorted, lines near $g \sim 2.0$ are expected. On the other hand, when the surroundings are distorted, large crystal fields are expected and lines in the low-field region of the spectrum are observed.

In the compound $CaAl_4O_7$, the Ca^{2+} ion exhibits a coordination number of seven. Within this coordination environment, the ionic radius of Ca^{2+} is 1.06 Å [44]. In contrast, when the Gd^{3+} ion is in a seven-fold coordination, its ionic radius is slightly smaller 1.0 Å. On the other hand, Al^{3+} ion resides in a fourfold coordination, possessing an ionic radius of 0.39 Å. Consequently, it is anticipated that the dopant Gd^{3+} ion will preferentially replace the Ca^{2+} ion rather than the Al^{3+} ion due to the smaller ionic radius of Al^{3+} compared to Ca^{2+}. Substitution of Ca^{2+} by Gd^{3+} ion would result in a positive charge accumulation. This charge imbalance can be compensated by the creation of Ca^{2+} vacancies or interstitial O_2^- ions near Gd^{3+} ions.

In the study of Eu^{3+}-doped $CaAl_4O_7$, Puchalska et al. [17] observed in their photoluminescence emission spectrum a red emission with a dominant emission line at about 612 nm (Excitation at 395 nm). They further identified two well-resolved emission spectral lines around 577.2 nm and 579.7 nm when experiments were carried out at liquid nitrogen temperatures (77 K). These results were interpreted in terms of two distinct sites of Eu^{3+} ion in the $CaAl_4O_7$ lattice. It was mentioned earlier that Ca^{2+} vacancies or interstitial O_2^- ions will be present near Eu^{3+} ions due to charge compensation. These can induce structural disorder around the dopant ion resulting in distinct Eu^{3+} sites in the host matrices. Based on the experimental results and conclusions from the above study on Eu^{3+} doped $CaAl_4O_7$, it is speculated that the $CaAl_4O_7$:Gd^{3+} phosphor may have two Gd^{3+} sites. The presence of a Ca^{2+} vacancy or an interstitial O_2^- ion in the vicinity of the Gd^{3+} ion may distort the environment around the dopant ion, making it experience a strong crystal field effect. Therefore, EPR signals appear in the low-field part of the spectrum [43]. This expectation is consistent with the observed EPR spectrum (see Fig. 10).

Apart from the low-field lines with relatively low intensity, two high-intensity EPR lines are observed at $g_{eff} \sim 2.16$ and 1.94 (Fig. 10), due to the presence of Gd^{3+} ions in undistorted Ca^{2+} sites. Charge-compensating defects are speculated to be in remote locations as far as these Ca^{2+} sites are concerned.

4. Conclusion

In this paper, samples of the $CaAl_4O_7$:Gd^{3+} phosphors with different concentrations of Gd ions were synthesized using the sol-gel technique. Detailed results of XRD, SEM, PL, and EPR of $CaAl_4O_7$:Gd^{3+} phosphors are reported. The XRD pattern confirms a stable single monoclinic phase with a C2/c space group. The variability of crystallite size in the range of 27–34 nm was observed for $CaAl_4O_7$:Gd^{3+} phosphor samples. SEM analysis revealed that the shape and size of the particles are somewhat irregular, and the formation of pores is visible in the crystalline grains. The vibrational stretching and bending modes of the AlO_4 units are considerably high in the 650-950 cm^{-1} frequency range in the FT-IR spectra, which facilitates the non-radiative relaxation process to the Gd^{3+}:^6P_J level for efficient UV-B emission of light. Upon excitation of 272 nm, a strong emission peak at 314 nm ($^6P_{7/2} \rightarrow {}^8S_{7/2}$) is observed together with a weak emission peak at 307 nm ($^6P_{5/2} \rightarrow {}^8S_{7/2}$). Concentration quenching of the emission of Gd^{3+}: $^6P_{7/2} \rightarrow {}^8S_{7/2}$ is observed which is caused by the transfer of energy non-radiatively, primarily via multipolar interactions between the Gd-Gd ions. Relatively strong EPR lines were observed around $g \sim 2.0$ along with small low-intensity signals in the low-field region of the spectrum. These lines suggest the presence of two distinct Gd^{3+} sites in the $CaAl_4O_7$ lattice. One of the sites is the originally undisturbed Ca^{2+} site, while the other is where its surroundings are disturbed by charge-compensating defects. The optimum activator ion concentration was estimated to be 3 mol%, based on the PL quenching data. In summary, the Gd ion is present in the 3+ state within the $CaAl_4O_7$ matrix. Further, the present results, though preliminary in nature, suggest that Gd^{3+} doped $CaAl_4O_7$ phosphors have the potential to be used as UV-B emitting phosphors for medical applications in the treatment of skin diseases.

Declaration of competing interest

The authors declare that they have no known competing financial interests or personal relationships that could have appeared to influence the work reported in this paper.

Acknowledgments

This work was supported by Konkuk University in 2021.

References

[1] Ji-Guang Li, Xiaodong Li, Xudong Sun, Ishigaki Takamasa, Monodispersed colloidal spheres for uniform Y_2O_3:Eu^{3+} red-phosphor particles and greatly enhanced luminescence by simultaneous Gd^{3+} doping, J. Phys. Chem. C 112 (31) (2008) 11707–11716.

[2] Sk Khaja Hussain, G. Seeta Rama Raju, Jae Su Yu, Synthesis and luminescent properties of $CaLa_2ZnO_5$:Ln (Ln:Tm^{3+} or Er^{3+}) phosphors, Ceram. Int. 41 (10) (2015) 13264–13270.

[3] C. Meric Guvenc, Yenal Yalcinkaya, Sercan Ozen, Hasan Sahin, Mustafa M. Demir, Gd^{3+}-doped α-$CsPbI_3$ nanocrystals with better phase stability and optical properties, J. Phys. Chem. C 123 (40) (2019) 24865–24872.

[4] Xin Li, Yang Cheng, Quansheng Liu, Xiaochun Wang, Xiaoyun Mi, Enhancement of luminescence properties of $SrAl_2Si_2O_8$:Eu^{3+} red phosphor, Ceram. Int. 46 (11) (2020) 17376–17382.

[5] Sanjay Kumar, A. Bandopadhyay, T.C. Alex, Rakesh Kumar, Influence of mechanical activation on the synthesis and hydraulic activity of calcium dialuminate, Ceram. Int. 32 (5) (2006) 555–560.

[6] Yoshikazu Suzuki, Tatsuki Ohji, Anisotropic thermal expansion of calcium dialuminate ($CaAl_4O_7$) simulated by molecular dynamics, Ceram. Int. 30 (1) (2004) 57–61.

[7] Yi Wu, Chao Hu Cheng, Bing Liu, Yu Hui Huang, Kai Xin Song, Crystal structure, vibrational spectroscopy, and microwave dielectric properties of $CaAl_4O_7$ ceramics with low permittivity, J. Mater. Sci. Mater. Electron. 31 (2020) 4520–4526.

[8] E. Boyko, L.G. Wisnyl, The optical properties and structures of $CaO.2Al_2O_3$ and $SrO.2Al_2O_3$, Acta Crystallogr. 11 (6) (1958) 444–445.

[9] J. Tang, J. Si, X. Fan, Y. Liu, G. Li, G. Cai, Tunable emission, energy transfer and thermal stability of Ce^{3+}, Tb^{3+} co-doped $Na_2BaCa(PO_4)_2$ phosphors, J. Rare Earths 40 (6) (2022) 878–887.

[10] R.R. Cui, X. Guo, X.Y. Gong, C.Y. Deng, Photoluminescence properties and energy transfer of novel orange–red emitting phosphors: $Ba_3Bi_2(PO_4)_4$:Sm^{3+}, Eu^{3+} for white light-emitting diodes, Rare Met. 40 (2021) 2882–2891.

[11] X. Huang, W. Zhang, X. Wang, J. Zhang, X. Gao, H. Du, Structure and luminescence investigation of Gd^{3+}-sensitized perovskite $CaLa_4Ti_4O_{15}$:Eu^{3+}: a novel red-emitting phosphor for high-performance white light-emitting diodes and plants lighting, J. Colloid Interface Sci. 608 (2022) 3204–3217.

[12] Z. Zhao, X. Wang, W. Zhang, L. Chen, H. Zhu, C. Qu, Effect of A^{3+} (A= Y, Bi) codoping on the enhancement of photoluminescence performance of $Li_5La_3Nb_2O_{12}$: Eu^{3+} red-emitting phosphor for white light-emitting diodes, Ceram. Int. 49 (2023) 25665–25674.

[13] T. Ma, X. Zhai, Y. Huang, M. Zhang, P. Li, Y. Du, Cerium ions crosslinked sodium alginate-carboxymethyl chitosan spheres with antibacterial activity for wound healing, J. Rare Earths 40 (9) (2022) 1407–1416.

[14] X. Zhang, L. Zhou, Q. Pang, J. Shi, M. Gong, Tunable luminescence and Ce^{3+}→ Tb^{3+}→ Eu^{3+} energy transfer of broadband-excited and narrow line red emitting Y_2SiO_5: Ce^{3+}, Tb^{3+}, Eu^{3+} phosphor, J. Phys. Chem. C 118 (2014) 7591–7759.

[15] Dongdong Jia, Jing Zhu, Boqun Wu, Luminescence and energy transfer in $CaAl_4O_7$: Tb^{3+}, Ce^{3+}, J. Lumin. 93 (2) (2001) 107–114.

[16] A. Kumar, R. Arun Kumar Suresh, Rama Ranjan Bhattacharjee, Synthesis and optical characterization of Tm^{3+} doped $CaAl_4O_7$ for near–UV LED-based white light, J. Lumin. 182 (2017) 130–136.

[17] M. Puchalska, Y. Gerasymchuk, E. Zych, Optical properties of Eu^{3+}-doped $CaAl_4O_7$ synthesized by the Pechini method, Opt. Mater. 32 (9) (2010) 1117–1122.

[18] Jungkyu Park, Gunha Kim, Young Jin Kim, Luminescent properties of $CaAl_4O_7$ powders doped with Mn^{4+} ions, Ceram. Int. 39 (2013) S623–S626.

[19] Vijay Singh, Sumedha Tamboli, S.J. Dhoble, Hoonil Jeong, Ultraviolet, vacuum ultraviolet excited photoluminescence study of sol-gel derived $CaAl_4O_7$:Tb^{3+} green emitting phosphor, Optik 213 (2020), 164375.

[20] M. Bakr, Ü.H. Kaynar, M. Ayvacikli, S. Benourdja, Y. Karabulut, A. Hammoudeh, N. Can, Synthesis and competitive luminescence quenching mechanism of $Ca_3Al_2O_6$: Ln^{3+} (Ln: Dy and Sm) phosphors, Mater. Res. Bull. 132 (2020), 111010.

[21] A.A. Bhat, S.A. Khanday, A.M. Ali, R. Tomar, Photoluminescence emission studies on a lanthanum-doped lead-free double halide perovskite, La:Cs_2SnCl_6, J. Phys. Chem. Lett. 14 (2023) 5004–5012.

[22] M. Ayvacikli, A. Canimoglu, L.E. Muresan, L.B. Tudoran, J.G. Guinea, Y. Karabulut, N. Can, Structural and luminescence effects of Ga co-doping on Ce-doped yttrium aluminate-based phosphors, J. Alloys Compd. 666 (2016) 447–453.

[23] Vijay Singh, S. Borkotoky, A. Murali, J.L. Rao, T.K. Gundu Rao, S.J. Dhoble, Electron paramagnetic resonance and photoluminescence investigation on ultraviolet-emitting gadolinium-ion-doped $CaAl_{12}O_{19}$ phosphors, Spectrochim. Acta Mol. Biomol. Spectrosc. 139 (2015) 1–6.

[24] G. Vijayaprasath, R. Murugan, Y. Hayakawa, G. Ravi, Optical and magnetic studies on Gd doped ZnO nanoparticles synthesized by co-precipitation method, J. Lumin. 178 (2016) 375–383.

[25] Yuhei Shimizu, Kazushige Ueda, Phase formation and UV luminescence of Gd^{3+} doped perovskite-type $YScO_3$, J. Solid State Chem. 242 (2016) 170–174.

[26] Vijay Singh, G. Sivaramaiah, J.L. Rao, S.H. Kim, Luminescence and electron paramagnetic resonance investigation on ultraviolet emitting Gd doped $MgAl_2O_4$ phosphors, J. Lumin. 143 (2013) 162–168.

[27] Vijay Singh, G. Sivaramaiah, J.L. Rao, S.H. Kim, Investigation of new UV-emitting, Gd-activated $Y_4Zr_3O_{12}$ phosphors prepared via combustion method, J. Lumin. 157 (2015) 82–87.

[28] Vijay Singh, G. Sivaramaiah, M. Mohapatra, J.L. Rao, N. Singh, M.S. Pathak, P. K. Singh, S.J. Dhoble, Probing the thermodynamic and magnetic properties of UV-B-emitting $GdAlO_3$ phosphors by ESR and optical techniques, J. Electron. Mater. 46 (2017) 1137–1144.

[29] A.D. Prokhorov, A.A. Prokhorov, L.F. Chernysh, V.P. Dyakonov, H. Szymczak, Temperature and pressure dependences of EPR spectra of Gd^{3+} ion doped in the $EuAl_3(BO_3)_4$ monocrystal, J. Magn. Magn Mater. 323 (11) (2011) 1546–1550.

[30] Ting Huang, Bo Jin, Ru Fang Peng, Cong Di Chen, Rong Zong Zheng, He Yi, Shi Jin Chu, Synthesis and characterization of [60] fullerene-glycidyl azide polymer and its thermal decomposition, Polymers 7 (5) (2015) 896–908.

[31] Brian Smith, The C= O bond, part VI: Esters and the rule of three, Spectroscopy 33 (7) (2018) 20–23.

[32] Aadil Ahmad Bhat, M. Burhanuz Zaman, Javied Hamid Malik, Khurshaid Ahmad Malik, Insaaf Assadullah, Radha Tomar, Facile way of making hydrothermally synthesized crystalline $SrSnO_3$ perovskite nanorods suitable for blue LEDs and spintronic applications, ACS Omega 6 (25) (2021) 16356–16363.

[33] Salah S. Musbah, Vesna Radojević, Ivana Radović, P.S. Uskoković, D.B. Stojanović, Miroslav Dramićanin, Radoslav Aleksić, Preparation, characterization and mechanical properties of rare-earth-based nanocomposites, J. Min. Metall. B Metall. 48 (2) (2012) 309–318.

[34] Stewart R. Dods, Hardick Oliver, Bob Stevens, Daniel G. Bracewell, Fabricating electrospun cellulose nanofibre adsorbents for ion-exchange chromatography, J. Chromatogr. A 1376 (2015) 74–83.

[35] BM Pradeep Kumara, K.H. Shivaprasada, R.S. Raveendrab, R. Hari Krishnac, B. M. Nagabhushanac, Adsorption of hazardous methylene blue from aqueous solution using combustion derived $CaAl_2O_4$ nanoparticles, Journal of Materials Science & Surface Engineering 4 (7) (2016) 492–495.

[36] Ruby Priya, O.P. Pandey, Photoluminescent enhancement with co-doped alkali metals in Gd_2O_3:Eu synthesized by co-precipitation method and Judd Ofelt analysis, J. Lumin. 212 (2019) 342–353.

[37] Ruby Priya, O.P. Pandey, Sanjay J. Dhoble, Review on the synthesis, structural and photo-physical properties of Gd_2O_3 phosphors for various luminescent applications, Opt Laser. Technol. 135 (2021), 106663.

[38] W.T. Carnall, P.R. Fields, K. Rajnak, Electronic energy levels of the trivalent lanthanide aquo ions. II. Gd^{3+}, J. Chem. Phys. 49 (10) (1968) 4443–4446.

[39] Thi Kim Chi Nguyen, Duy Hung Nguyen, Tan Vinh Le, Thanh Vu Tran, Chi Nguyen Vo, Thi Kim Trung Pham, Luminescence properties of Mn^{4+}-doped $CaAl_2O_4$ as a red emitting phosphor for white LEDs, Vietnam Journal of Science, Technology and Engineering 63 (3) (2021) 3–7.

[40] V. Rama Devi, B. Vijaya Kumar, Radha Velchuri, Palla Suresh, G. Ravi, M. Vithal, Effect of crystallite size on electron spin resonance of Gd^{3+} and luminescence of Eu^{3+} doped in La $_6WO_{12}$, Indian J. Eng. Mater. Sci. 19 (2012) 204–208.

[41] Hakyung Jeong, N. Singh, M.S. Pathak, S. Watanabe, T.K. Gundu Rao, Vikas Dubey, Vijay Singh, Investigations of the ESR and PL characteristics of ultraviolet-emitting gadolinium-doped $ZnMgAl_{10}O_{17}$ phosphors, Optik 157 (2018) 1199–1206.

[42] D.W. Goodwin, A.J. Lindop, The crystal structure of $CaO.2Al_2O_3$, Acta Crystallogr. B Struct. Crystallogr. Cryst. Chem. 26 (9) (1970) 1230–1235.

[43] C.M. Brodbeck, L.E. Iton, The EPR spectra of Gd^{3+} and Eu^{2+} in glassy systems, J. Chem. Phys. 83 (9) (1985) 4285–4299.

[44] Robert D. Shannon, Revised effective ionic radii and systematic studies of interatomic distances in halides and chalcogenides, Acta Crystallogr. Sect. A Cryst. Phys. Diffr. Theor. Gen. Crystallogr. 32 (5) (1976) 751–767.